International Journal of Pharmacology

Int. J. Pharmacol. **2025**; 21(8): 46592
https://doi.org/10.31083/IJP46592

Research Article

Adropin Alleviates High-Glucose-Induced Cardiomyocyte Apoptosis *In Vitro* via the Modulation of Mitophagy and Mitochondrial Dynamics

Mao Liu[1,*,†], Pengfei Chen[1,†], Siliang Wang[1], Gang Zeng[2], Zhan Lv[1]

[1]Department of Cardiology, Cardiovascular Research Center, Affiliated Hospital of North Sichuan Medical College, 637000 Nanchong, Sichuan, China
[2]Department of Cardiology, Guang'an District People's Hospital, 638550 Guang'an, Sichuan, China
*Correspondence: doc_mliu@sina.cn (Mao Liu)
†These authors contributed equally.

Academic Editor: Mehmet Ozaslan
Submitted: 15 September 2025 Revised: 4 November 2025 Accepted: 21 November 2025 Published: 22 December 2025

Abstract

Background and Objective: Diabetic cardiomyopathy (DbCM) is a serious complication of diabetes. Adropin (ADR), a 76-amino acid peptide encoded by the *Energy homeostasis associated* (*Enho*) gene, plays a crucial role in energy homeostasis. However, the effects of (*Enho*) on cardiomyocytes (CMs) apoptosis under hyperglycemic conditions and the associated mechanisms remain poorly understood. Thus, this study aimed to investigate the protective effects of ADR against high glucose-induced CM apoptosis and elucidate the underlying mechanisms involving mitophagy and mitochondrial dynamics. **Materials and Methods**: Neonatal rat CMs were cultured *in vitro* and divided into three groups: control (CMs), high glucose condition (HGLc; CMs + HGLc), and HGLc with ADR treatment (CMs + HGLc + ADR). Cell viability was assessed using the MTT assay, while apoptosis was quantified by flow cytometry. Lysosomal activity was evaluated via fluorescent probes, and autophagic flux was measured using the monomeric Red Fluorescent Protein-enhanced Green Fluorescent Protein-Microtubule-associated protein 1 light chain 3 (mRFP-eGFP-LC3) dual-fluorescence system. The expression of Proteins invoved in mitophagy and mitochondrial dynamics was analyzed by Western blotting. **Results**: High glucose exposure significantly reduced CM viability, increased apoptosis, and impaired mitochondrial membrane potential and autophagy ($p < 0.05$ vs. the controls group). These effects were accompanied by downregulation of sequestosome 1 (p62), PTEN-induced kinase 1 (PINK1), Parkin, Mitofusin 1 (Mfn1), and Mitofusin 2 (Mfn2), and upregulation of Dynamin-related protein 1 (Drp1) . ADR treatment attenuated these abnormalities, restoring viability, reducing apoptosis, and improving mitochondrial function and autophagy ($p < 0.05$ vs. CMs + HGLc group). Notably, ADR upregulated p62, PINK1, Parkin, Mfn1 and Mfn2 while suppressing Drp1 expression ($p < 0.05$ vs CMs + HGLc group). **Conclusion**: ADR mitigates high glucose-induced CMs apoptosis by enhancing mitophagy and restoring mitochondrial dynamics, suggesting that ADR treatment offers therapeutic potential for DbCM.

Keywords: adropin; mitochondrial dynamics; mitophagy; cardiomyocyte; diabetic cardiomyopathies

1. Introduction

Diabetes has emerged as one of the most severe and prevalent diseases in modern society. Globally, approximately 10.5% of individuals aged 20–79 are affected by diabetes, and its incidence continues to rise [1]. Diabetes significantly increases cardiovascular risks, with diabetic patients facing more than double the risk of heart failure compared to non-diabetic individuals. Moreover, the prevalence of diabetes among heart failure patients is notably high [2,3].

Diabetic cardiomyopathy (DbCM), a severe complication of diabetes, is characterized by structural and functional damage to the heart, including ventricular dysfunction, myocardial hypertrophy, cardiomyocytes (CMs) apoptosis, interstitial fibrosis, and metabolic dysregulation [4,5]. These pathophysiological changes drive cardiac remodeling, reduce cardiac output, and ultimately lead to heart failure and death [6]. Due to the subtlety of early symptoms and the lack of effective treatments, DbCM remains challenging to diagnose and manage [7,8]. Thus, proactive and comprehensive strategies for early prevention and treatment are critical.

Adropin (ADR) is a 76-amino acid peptide encoded by the *Energy homeostasis associated* (*Enho*) gene, is expressed in multiple organs, including the heart, liver, and brain [9]. Its functional exertion mainly relies on binding to relevant receptors including G protein-coupled receptor 19 (GPR19) [10]. And it is closely associated with metabolic disorders such as hypertension, obesity, and diabetes [11,12]. ADR plays a vital role in energy homeostasis, partly by enhancing insulin signaling pathways, promoting glucose uptake in tissues, and inhibiting hepatic glucose production [12,13].

In CMs, ADR activates the G protein-coupled receptor-Mitogen-activated protein kinase-Pyruvate dehydrogenase kinase 4 pathway (GPCR-MAPK-PDK4) pathway, downregulating mitochondrial pyruvate dehydrogenase kinase 4 (PDK4) expression [14]. This reduces inhibitory phosphorylation of pyruvate dehydrogenase, facilitating glucose utilization [12,15]. Additionally, ADR low-

ers low-density lipoprotein levels, improving lipid profiles and cardiovascular health [16]. It also serves as a biomarker for heart disease, with studies indicating a correlation between plasma ADR levels and heart failure severity [17,18].

Previous research demonstrated that ADR reduces myocardial fibrosis and improves remodeling in diabetic rats, highlighting its therapeutic potential for DbCM [19]. However, its effects on CMs apoptosis under high-glucose conditions and the underlying mechanisms remain unclear. This study investigates ADR's role in mitigating high glucose-induced CMs apoptosis, focusing on mitophagy and mitochondrial dynamics.

2. Materials and Methods

2.1 Materials and Reagents

Fetal bovine serum (FBS) was obtained from Hyclone (Logan, UT, USA). DMEM/F12 medium and trypsin were purchased from GIBCO (Grand Island, NE, USA), while penicillin-streptomycin was sourced from Sigma-Aldrich (St. Louis, MO, USA). Other reagents, including Ponceau S, Tris-Buffered Saline with Tween 20 (TBST), acrylamide, SDS, PMSF, and protein membrane regeneration solution, were acquired from Beijing Bio-Lab Technology Co., Ltd. (Beijing, China). Radio-Immunoprecipitation Assay (RIPA) lysis buffer, Lyso-Tracker Red, and the JC-1 mitochondrial membrane potential detection kit were purchased from Beyotime Biotechnology (Shanghai, China). The MTT assay kit was obtained from Solarbio (Beijing, China), and the monomeric Red Fluorescent Protein-enhanced Green Fluorescent Protein-Microtubule-associated protein 1 light chain 3 (mRFP-GFP-LC3) adenovirus was procured from Hanbio Biotechnology Co., Ltd. Antibodies against Dynamin-related protein 1 (Drp1) (8570), Mitofusin 2 (Mfn2) (9482), sequestosome 1 (p62) (5114) and Parkin (4211) were purchased from Cell Signaling Technology (Boston, MA, USA), and antibodies against PTEN-induced kinase 1 (PINK1) (ab186303) and Mitofusin 1 (Mfn1) (ab126575) were from Abcam (Cambridge, UK). ADR was supplied by Shanghai Lianmai Bioengineering Co., Ltd., and the Annexin V/PI dual-staining kit was obtained from Invitrogen (Carlsbad, CA, USA).

2.2 Experimental Instruments

Key instruments included a Thermo Scientific FORMA 700 ultra-low temperature freezer (Waltham, MA, USA), a Zhongke Meiling YC-300L pharmaceutical storage cabinet (Hefei, Anhui, China), and a Thermo Electron Forma 3111 CO_2 incubator (Waltham, MA, USA). Protein analysis was performed using a Bio-Rad Trans-Blot® transfer system (1704150) (Hercules, California, USA) and Criterion™ electrophoresis chamber (1656001) (Hercules, CA, USA). Imaging was conducted with a Tanon 6600 chemiluminescent system (Shanghai, China) and a Zeiss LSM 900 confocal microscope (Jena, Baden-Württemberg, Germany). Flow cytometry was performed using a Beckman Coulter DxFLEX flow cytometer (Brea, CA, USA).

2.3 Cell Extraction and Culture

Primary neonatal rat CMs were isolated from apical ventricular tissue via enzymatic digestion with 1 g/L trypsin, followed by overnight incubation at 4 °C. Most of the trypsin was then discarded, and an equal volume of complete medium was added to terminate the digestion. After removing the supernatant, 0.8 g/L type II collagenase was added, and the mixture was digested with shaking in a 37 °C water bath for 8–10 minutes before collecting the supernatant. This digestion step was repeated 3–4 times, and the supernatants from each round were combined. Following centrifugation, the non-adherent cell suspension was aspirated and transferred to a culture dish, after which 5-Bromo-2'-deoxyuridine (BrdU) was added to label non-cardiomyocytes and flow cytometry was subsequently performed for cell sorting to enrich cardiomyocytes. Cells were cultured in DMEM/F12 medium supplemented with 10% FBS and maintained in a humidified incubator at 37 °C under 5% CO_2. After cultivation, the CMs were fixed, permeabilized, and blocked, followed by sequential incubation with the cardiac-specific α-actinin antibody and fluorescent secondary antibody. After DAPI nuclear staining, CMs were identified by observing specific cytoplasmic fluorescence with characteristic sarcomeric striations under a fluorescence microscope. Mycoplasma contamination was excluded using the PCR method. For the experiments, CMs at the logarithmic growth phase (2nd–3rd passages) were used. This study was conducted under the supervision of the Ethics Committee of North Sichuan Medical College.

2.4 Experimental Group

Three groups were set in this study. Cells in CMs group were incubated in normal medium (DMEM/F-12 containing 17.5 mmol/L D-glucose) for 48 hours. Cells in CMs + high glucose condition (HGLc) group were incubated in DMEM/F-12 medium containing 33.0 mmol/L D-glucose for 48 hours. Cells in CMs + HGLc + ADR group were incubated in DMEM/F-12 medium containing 33.0 mmol/L D-glucose and 5 µg/mL (0.66 µmol/L) ADR for 48 hours.

2.5 MTT

CMs in the logarithmic growth phase were cultured under standard conditions (37 °C, 5% CO_2) until reaching 90% confluence. Prior to treatment, cells were synchronized by serum starvation (serum-free DMEM/F12 medium, 2 h). Following 48 h of experimental treatments, the culture medium was carefully aspirated. For the assay, 90 µL of fresh medium was added to each well, followed by 10 µL of MTT solution (5 mg/mL in PBS). Cells were then incubated for 4 h (37 °C, 5% CO_2) to allow formazan crystal

formation. After incubation, the supernatant was removed, and 110 µL of DMSO (or appropriate formazan solubilization solution) was added to each well. Plates were gently agitated on an orbital shaker for 10 min to ensure complete crystal dissolution. Finally, the optical density was measured at 490 nm using a microplate reader (BioTek Synergy H1, Winooski, VT, USA), with reference wavelength set at 630 nm to account for background absorbance.

2.6 Cell Apoptosis

CMs were harvested, washed with ice-cold PBS (4 °C), and centrifuged at 1000 ×g for 5 min at 4 °C. After discarding the supernatant, cells were resuspended in 1× Annexin binding buffer at a density of 1×10^6 cells/mL. Subsequently, 5 µL Alexa Fluor 488 Annexin V and 1 µL propidium iodide (PI, 100 µg/mL) were added to each sample, followed by a 15-min incubation in the dark. Apoptotic rates were quantified using flow cytometry.

2.7 Mitochondrial Membrane Potential

JC-1 dye was diluted in staining buffer and vortexed thoroughly to prepare the working solution. Collected cells were resuspended in 0.5 mL culture medium, mixed with 0.5 mL JC-1 working solution, and incubated at 37 °C for 20 min. After centrifugation (300 ×g, 3 min), the pellet was washed twice with JC-1 buffer and resuspended in 1× buffer. Mitochondrial depolarization (green/red fluorescence ratio) was analyzed by flow cytometry.

2.8 Lysosomal Red Fluorescent Probe Staining

CMs in logarithmic growth phase were seeded in 6-well plates (50–70% confluency). Cells were washed with PBS and incubated with 50 nM Lyso-Tracker Red (37 °C, 30 min, dark), followed by Hoechst 33342 nuclear counterstaining (20 min). After PBS washes, coverslips were mounted, and lysosomal fluorescence was captured using a Zeiss LSM 900 confocal microscope. The fluorescence intensity was analyzed by Image J software (Bethesda, MD, USA).

2.9 Dual Fluorescence mRFP-eGFP-LC3 Self-Indicating System

Cells (1×10^6/well) were seeded 24 h prior to infection with mRFP-eGFP-LC3 adenovirus (50 µL/well, 70% confluency). After 24 h incubation (37 °C, 5% CO_2), cells were permeabilized with 0.3% Triton X-100 (10 min), washed with PBS, and imaged at 630× magnification. Autophagosomes (yellow puncta) and autolysosomes (red puncta) were quantified across three random fields per sample using Image J software.

2.10 Western Blot

Neonatal rats (provided by Changzhou Kavens Laboratory Animal Co., Ltd.) were subjected to thoracotomy under sterile conditions to extract the apical tissue. Treated cells were lysed with 400 µL of RIPA lysis buffer on ice for 30 minutes. The lysate was centrifuged at 12,000 ×g for 15 minutes at 4 °C, and the supernatant was collected for protein quantification using the BCA assay (Bio-Rad kit). A total of 20–30 µg of protein was loaded per lane, separated by SDS-PAGE gel electrophoresis, and then transferred to a Polyvinylidene Fluoride (PVDF) membrane. The membrane was incubated with primary antibodies (Drp1/Mfn2/P62/PINK1/Parkin at a dilution of 1:1000, Mfn1 at a dilution of 1:2000) at 4 °C overnight. After washing the membrane with TBST, it was incubated with secondary antibodies at a dilution of 1:5000 at room temperature for 1 hour. Following incubation with horseradish peroxidase (HRP)-conjugated secondary antibodies, protein bands were visualized using the Tanon 6600 chemiluminescence system. The optical density of the bands was analyzed using Image Pro Plus 6.0 software (Media Cybernetics, Silver Spring, MD, US), and the relative protein expression levels were calculated with GAPDH/β-actin as internal references.

2.11 Statistical Analysis

Data were presented as group mean and its standard error (mean ± SEM). One-way analysis of variance (ANOVA) followed by the least significant difference (LSD) post hoc test was used for the statistical analysis of the difference between multiple groups. If the conditions are not met, non-parametric tests should be chosen instead. $p < 0.05$ is regarded as statistically significant. All statistical analyses were performed in IBM SPSS Statistics for Windows version 20.0 (IBM Corp, Armonk, NY, USA).

3. Results

3.1 ADR Preserves CMs Viability

MTT assays revealed that high glucose exposure significantly reduced CM viability compared to CMs group (62.94 ± 3.22% vs 100 ± 1.57%, $p < 0.05$). ADR treatment partially restored viability (77.74 ± 3.56% vs 62.94 ± 3.22%, $p < 0.05$), though remained lower than CMs group ($p < 0.05$, Fig. 1).

3.2 ADR Attenuates High Glucose-Induced CMs Apoptosis

Flow cytometry analysis demonstrated a 3.6-fold increase in apoptosis under high glucose conditions (27.55 ± 0.64% vs 7.67 ± 1.01%, $p < 0.05$). ADR intervention significantly reduced apoptosis by 32.6% (18.56 ± 2.92% vs 27.55 ± 0.64%, $p < 0.05$), yet remained elevated versus control ($p < 0.05$, Fig. 2).

3.3 ADR Restores Mitochondrial Membrane Potential

As shown in Fig. 3, JC-1 staining showed high glucose-induced mitochondrial depolarization, evidenced by increased green/red fluorescence ratio (20.37 ± 1.87%

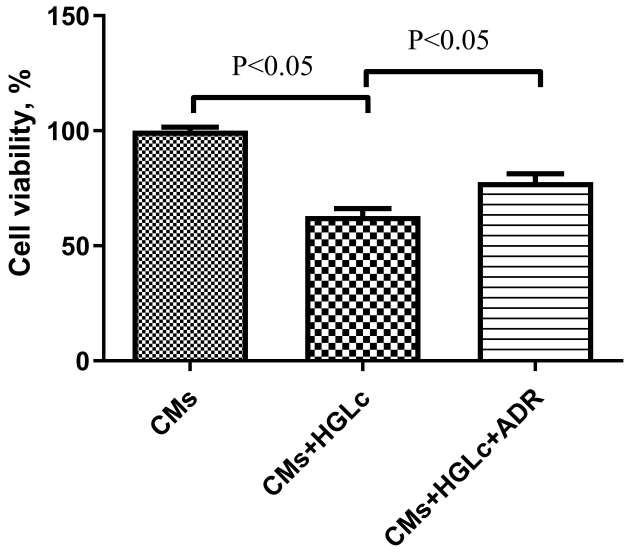

Fig. 1. Effect of ADR on viability of CMs. Cell viability of each group was detected using the 3-(4,5-Dimethylthiazol-2-yl)-2,5-Diphenyltetrazolium Bromide assay (MTT) assay. Compared to cardiomyocytes (CMs) group, cell viability decreased in CMs + high glucose condition (HGLc) group. Compared to CMs + HGLc group, it increased in CMs + HGLc + adropin (ADR) group. N = 3, it represents three independent biological replicates, with three technical replicates per experiment. Values were expressed as mean ± standard deviation.

vs 4.79 ± 0.91%, $p < 0.05$). ADR treatment significantly improved mitochondrial potential (11.83 ± 1.67%, $p < 0.05$ vs CMs + HGLc group).

3.4 ADR Enhances Lysosomal Activity

LysoTracker Red fluorescence intensity decreased by 76% under high glucose (0.24 ± 0.02% vs 1.00 ± 0.02%, $p < 0.05$). ADR treatment increased fluorescence intensity 3.1-fold (0.74 ± 0.04% vs 0.24 ± 0.02%, $p < 0.05$), indicating restored lysosomal function (Fig. 4).

3.5 Effect of ADR on Autophagy in CMs

The mRFP-eGFP-LC3 system revealed that high glucose reduced autolysosomes (red puncta) by 54% (31.11 ± 1.13% vs 67.47 ± 8.82%), decreased autophagosomes (yellow puncta) by 58% (50.90 ± 1.61% vs 120.15 ± 6.14%) ($p < 0.05$ for both). ADR treatment significantly increased red puncta by 46% (45.44 ± 2.36% vs 31.11 ± 1.13%) and yellow puncta by 51% (76.64 ± 6.78% vs 50.90 ± 1.61%) versus CMs + HGLc group ($p < 0.05$, Fig. 5).

3.6 ADR Regulates Mitophagy-Related Proteins in CMs

As shown in Fig. 6, western blot analysis demonstrated that high glucose reduced p62 by 50% (0.43 ± 0.01% vs 0.86 ± 0.18%), decreased PINK1 by 32% (0.62 ± 0.07% vs 0.91 ± 0.03%), lowered Parkin by 49% (0.37 ± 0.06% vs 0.72 ± 0.02%) ($p < 0.05$ for all). ADR treatment significantly increased p62 by 60% (0.69 ± 0.07% vs 0.43 ± 0.01% , $p < 0.05$), PINK1 by 27% (0.79 ± 0.04% vs 0.62 ± 0.07%, $p < 0.05$), Parkin by 51% (0.56 ± 0.04% vs 0.37 ± 0.06%, $p < 0.05$) versus high glucose.

3.7 ADR Modulates Mitochondrial Dynamics Proteins in CMs

As shown in Fig. 7, high glucose exposure reduced Mfn1 by 47% (0.57 ± 0.04% vs control 1.08 ± 0.12%), decreased Mfn2 by 52% (0.53 ± 0.03% vs 1.11 ± 0.13%), increased Drp1 by 2.1-fold (1.58 ± 0.22% vs 0.74 ± 0.08%) ($p < 0.05$). However, ADR treatment increased Mfn1 by 61% (0.92 ± 0.07% vs 0.57 ± 0.04%, $p < 0.05$), elevated Mfn2 by 45% (0.77 ± 0.05% vs 0.53 ± 0.03%, $p < 0.05$), and reduced Drp1 by 35% (1.02 ± 0.14% vs 1.58 ± 0.22%, $p < 0.05$) versus CMs + HGLc group.

4. Discussion

The results of this study indicated that the CMs + HGLc group exhibited a decreased survival rate of CMs, increased the green to red fluorescence ratio of mitochondrial membrane JC-1, decreased mitochondrial membrane potential and increased apoptosis rate of CMs. However, with the intervention of ADR, an increase in CMs survival rate, a decrease in the green to red fluorescence ratio of mitochondrial membrane JC-1, an increase in mitochondrial membrane potential and a decrease in CMs apoptosis rate were observed.

Mitochondrial function exhibits a strong correlation with CMs apoptosis [20]. Mitochondria are highly dynamic organelles that occupy nearly 1/3 of the volume of cardiac cells and are the "powerhouse" of the heart [21]. The precisely regulated balance between mitochondrial fission and fusion processes, collectively referred to as mitochondrial dynamics [22]. When cells undergo metabolic or environmental stress, they maintain their shape, distribution, and size through fusion, fission, and mitophagy [23]. In cardiac metabolic pathologies, proper mitochondrial dynamics and mitophagy contribute significantly to enhanced insulin sensitivity, optimized metabolite utilization, suppressed inflammatory responses, attenuated apoptotic pathways, endothelial protection, and prevention of ventricular remodeling [24]. Mitochondrial swelling and mitochondrial dysfunction may ultimately lead to left ventricular dysfunction and pathological cardiac hypertrophy [25].

ADR, a peptide encoded by the *Enho* gene, is closely associated with various metabolic diseases [12]. A study has reported that ADR can improve myocardial cell apoptosis in a mouse model of radiation-induced myocardial injury [9]. It was also observed that ADR alleviates ischemia/reperfusion injury in mouse myocardial cells [26]. The mechanism may be related to the regulation of apoptosis through the activation of downstream target Glycogen Synthase Kinase 3 Beta (GSK3β) [26,27]. In the DbCM animal model, our previous study found that ADR can im-

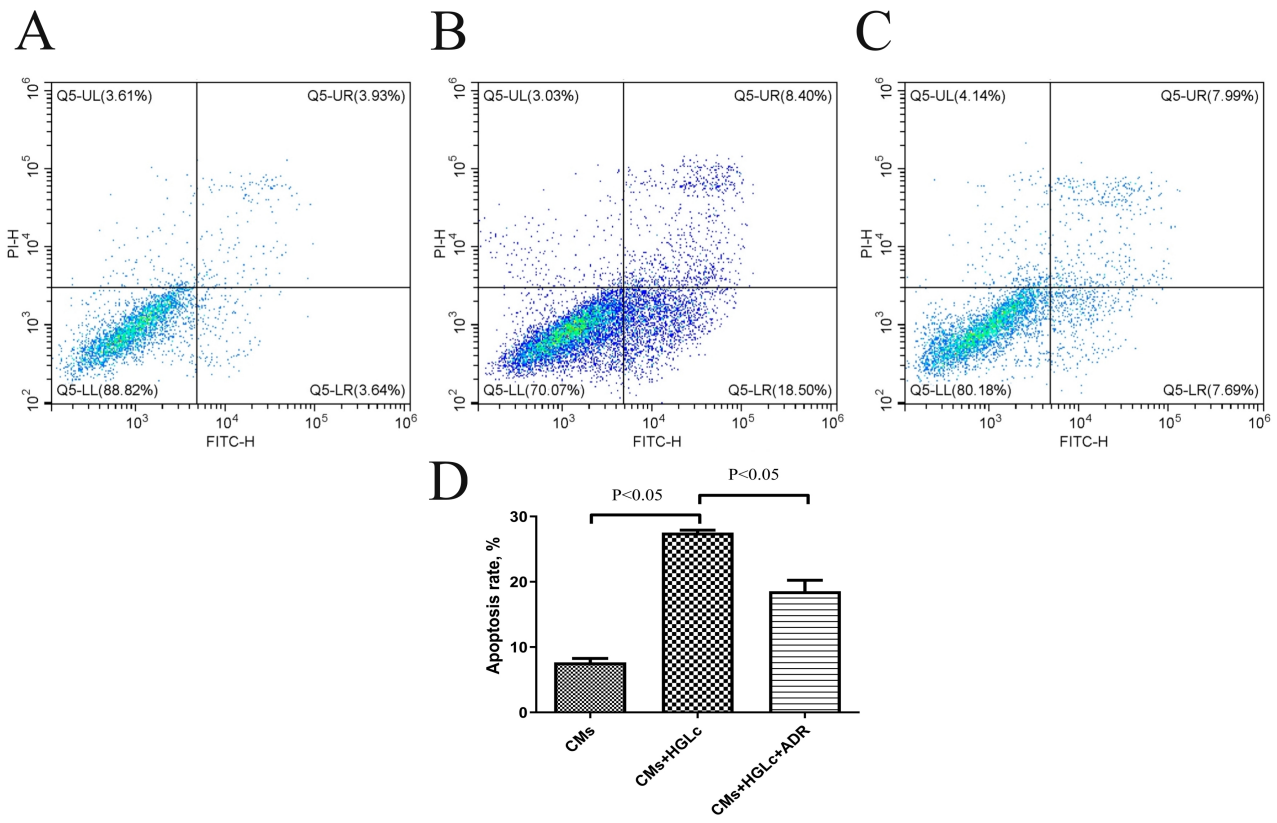

Fig. 2. Effect of ADR on apoptosis of CMs. Cell apoptosis was detected by flow cytometry. (A) Flow cytometry scatter plot of apoptosis in CMs group (FITC-H, fluorescence channel for apoptotic marker; PI-H, propidium iodide staining channel). The quadrant percentages are as follows: viable cells (Q5-LL): 88.82%, early apoptotic cells (Q5-LR): 3.64%, late apoptotic cells (Q5-UR: 3.93%), necrotic cells (Q5-UL: 3.61%). (B) Flow cytometry scatter plot of CMs after high glucose condition (HGLc) treatment. The quadrant percentages are as follows: viable cells (Q5-LL): 70.07%, early apoptotic cells (Q5-LR): 18.50%, late apoptotic cells (Q5-UR: 8.40%), necrotic cells (Q5-UL: 3.03%). (C) Flow cytometry scatter plot of CMs co-treated with HGLc and adropin (ADR). The quadrant percentages are as follows: viable cells (Q5-LL): 80.18%, early apoptotic cells (Q5-LR): 7.69%, late apoptotic cells (Q5-UR: 7.99%), necrotic cells (Q5-UL: 4.14%). (D) Compared to CMs group, the apoptosis rate increased in CMs + HGLc group ($p < 0.05$). Compared to CMs + HGLc group, it decreased in CMs + HGLc + ADR group ($p < 0.05$). N = 3, it represents three independent biological replicates, with three technical replicates per experiment. Values were expressed as mean ± standard deviation.

prove ventricular remodeling in DbCM rats [19]. The experiments in this study were conducted from the cellular level. The results indicated that ADR can reduce the apoptosis rate, enhance autophagy of CMs under high glucose conditions, providing supporting evidence for the role of ADR in improving ventricular remodeling in DbCM.

The PINK1-Parkin pathway is an important pathway for initiating mitophagy. PINK1 is a cytosolic serine/threonine kinase, which is rapidly degraded by mitochondrial proteases in the inner membrane of healthy mitochondria [28]. When mitochondria are damaged, changes in the mitochondrial membrane potential inhibit the degradation of PINK1 by proteases [23]. The accumulated PINK1 recruits Parkin to the outer membrane of the mitochondria [29]. Activated Parkin induces ubiquitination of proteins on the outer mitochondrial membrane, leading to the occurrence of autophagy [28]. This study found that mitophagy of CMs is reduced under high glucose conditions. In experiments extracting mitophagy-related proteins, the expression of PINK1, Parkin, and P62 proteins involved in PINK1-Parkin pathway was decreased in the CMs + HGLc group, while they were increased in the ADR intervention group. The mechanism may be related to the regulation of the PINK1-Parkin pathway.

Mitochondrial dynamics are related to the occurrence of CMs apoptosis [30]. Mitochondrial fusion proteins and mitochondrial fission proteins are of great significance to mitochondrial homeostasis. An imbalance between mitochondrial fusion and fission will have adverse effects on mitochondrial homeostasis [31], which causes the accumulation of damaged organelles produce ROS and progressive heart failure [32]. Excessive or absent expression of

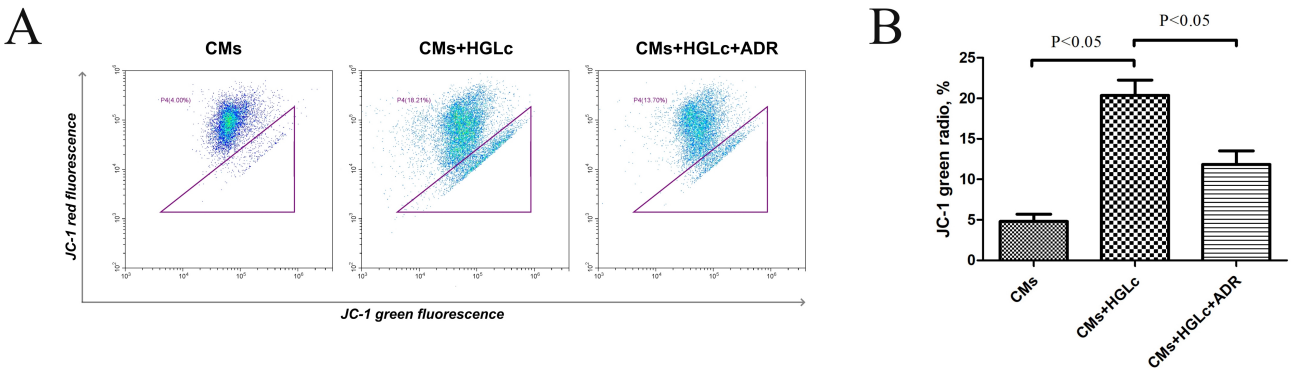

Fig. 3. Effect of ADR on mitochondrial membrane potential of CMs. Mitochondrial membrane potential was detected by flow cytometry. (A) JC-1 fluorescence scatter plots of different groups (JC-1 red fluorescence: ordinate; JC-1 green fluorescence: abscissa; P4: region of cells with decreased mitochondrial membrane potential). The percentage of P4 region in each group is as follows: cardiomyocytes (CMs) group: 4.00%; CMs + high glucose condition (HGLc) group: 18.21%; CMs + HGLc + adropin (ADR) group: 13.70%. (B) Compared to CMs group, the green radio increased in CMs + HGLc group ($p < 0.05$). Compared to CMs + HGLc group, it decreased in CMs + HGLc + ADR group ($p < 0.05$). N = 3, it represents three independent biological replicates, with three technical replicates per experiment. Values were expressed as mean ± standard deviation.

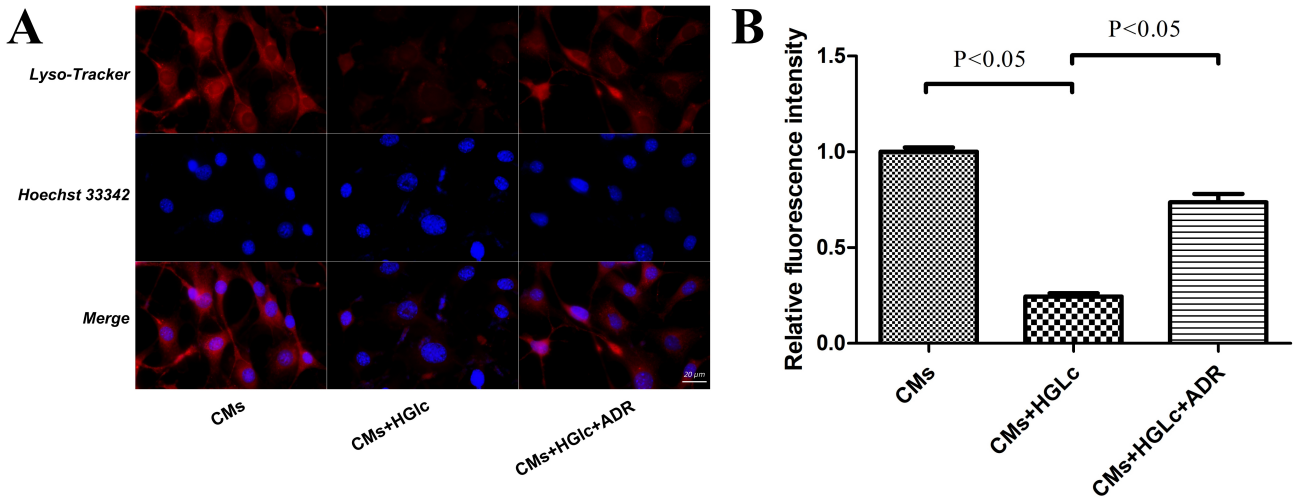

Fig. 4. Effect of ADR on lysosomes in CMs. Lysosomal activity was detected by lysosomal red probe. (A) Fluorescence images of cardiomyocytes (CMs) in different groups (Lyso-Tracker: red fluorescence, labeling lysosomes; Hoechst 33342: blue fluorescence, labeling cell nuclei; Merge: merged images of red and blue fluorescence). From left to right: CMs group, CMs + high glucose condition (HGLc) group, CMs + HGLc + adropin (ADR) group. The scale bar: 20 μm. (B) Compared to CMs group, the fluorescence intensity decreased in CMs + HGLc group. Compared to CMs + HGLc group, it increased in CMs + HGLc + ADR group. N = 3, it represents three independent biological replicates, with three technical replicates per experiment. Values were expressed as mean ± standard deviation.

Drp1 will affect mitochondrial homeostasis [33]. Many studies have shown that Drp1 protein expression is upregulated and plays a role in mediating programmed cell death necrosis in pathological conditions in the heart [34,35]. It's reported that the ablation of Drp1 interrupts mitochondrial fission and significantly increases Parkin levels, enhancing Parkin-mediated mitophagy [36]. Our previous animal experiments in DbCM rats also indicated that the expression of Mfn1 and Mfn2 in myocardial tissue increased, and the expression of Drp1 decreased after the intervention of ADR [19]. This study confirmed the results at cellular level. In high glucose stimulation, Mfn1 and Mfn2 proteins in CMs were decreased. The Drp1 protein and fragmented mitochondria were increased. However, after the intervention with ADR, the mitochondrial abnormal fission decreased, and mitochondrial function was improved. Therefore, combining the *in vivo* and *in vitro* experiments, it was found that ADR can reduce CMs apoptosis and improve DbCM ventricular remodeling by regulating mitochondrial dynamics and mitophagy.

This study has both strengths and limitations. By investigating ADR's effects on CMs at the cellular level,

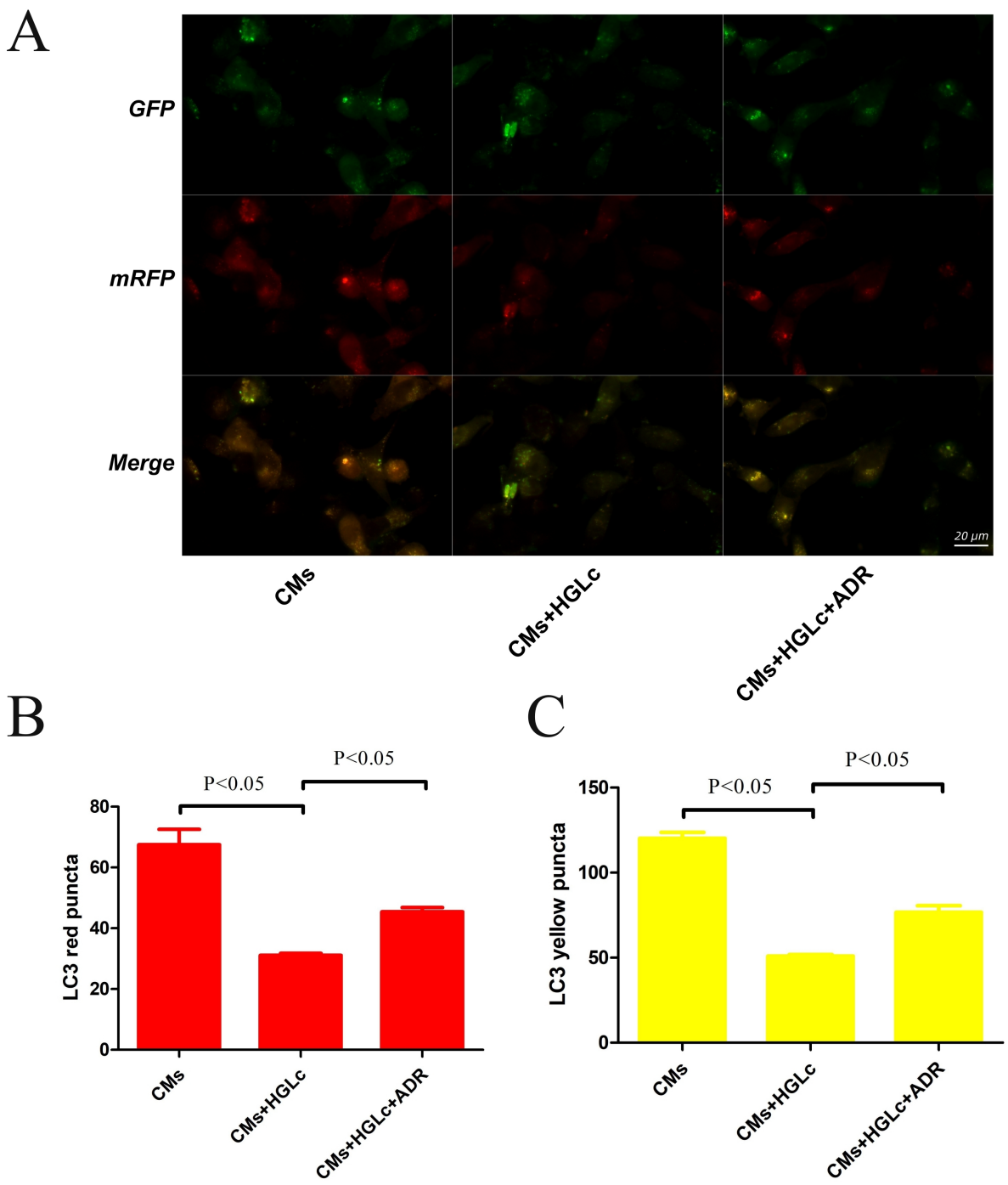

Fig. 5. Effect of ADR on autophagy in CMs. Autophagy in cardiomyocytes (CMs) was detected using the monomeric Red Fluorescent Protein-enhanced Green Fluorescent Protein-Microtubule-associated protein 1 light chain 3 (mRFP-GFP-LC3) system. (A) Fluorescence images of mRFP-GFP-LC3 (GFP: green fluorescence; mRFP: red fluorescence; Merge: merged images; yellow puncta in Merge represent autophagosomes). From left to right: CMs group, CMs + high glucose condition (HGLc) group, CMs + HGLc + adropin (ADR) group. The scale bar: 20 μm. (B) Quantitative analysis chart of LC3 red puncta (representing autophagosome precursors). Compared with the CMs group, the number of LC3 red puncta in the CMs + HGLc group was significantly decreased ($p < 0.05$); compared with the CMs + HGLc group, the number of LC3 red puncta in the CMs + HGLc + ADR group was significantly increased ($p < 0.05$). (C) Quantitative analysis chart of LC3 yellow puncta (representing mature autophagosomes). Compared with the CMs group, the number of LC3 yellow puncta in the CMs + HGLc group was significantly decreased ($p < 0.05$); compared with the CMs + HGLc group, the number of LC3 yellow puncta in the CMs + HGLc + ADR group was significantly increased ($p < 0.05$). N = 3, it represents three independent biological replicates, with three technical replicates per experiment. Values were expressed as mean ± standard deviation.

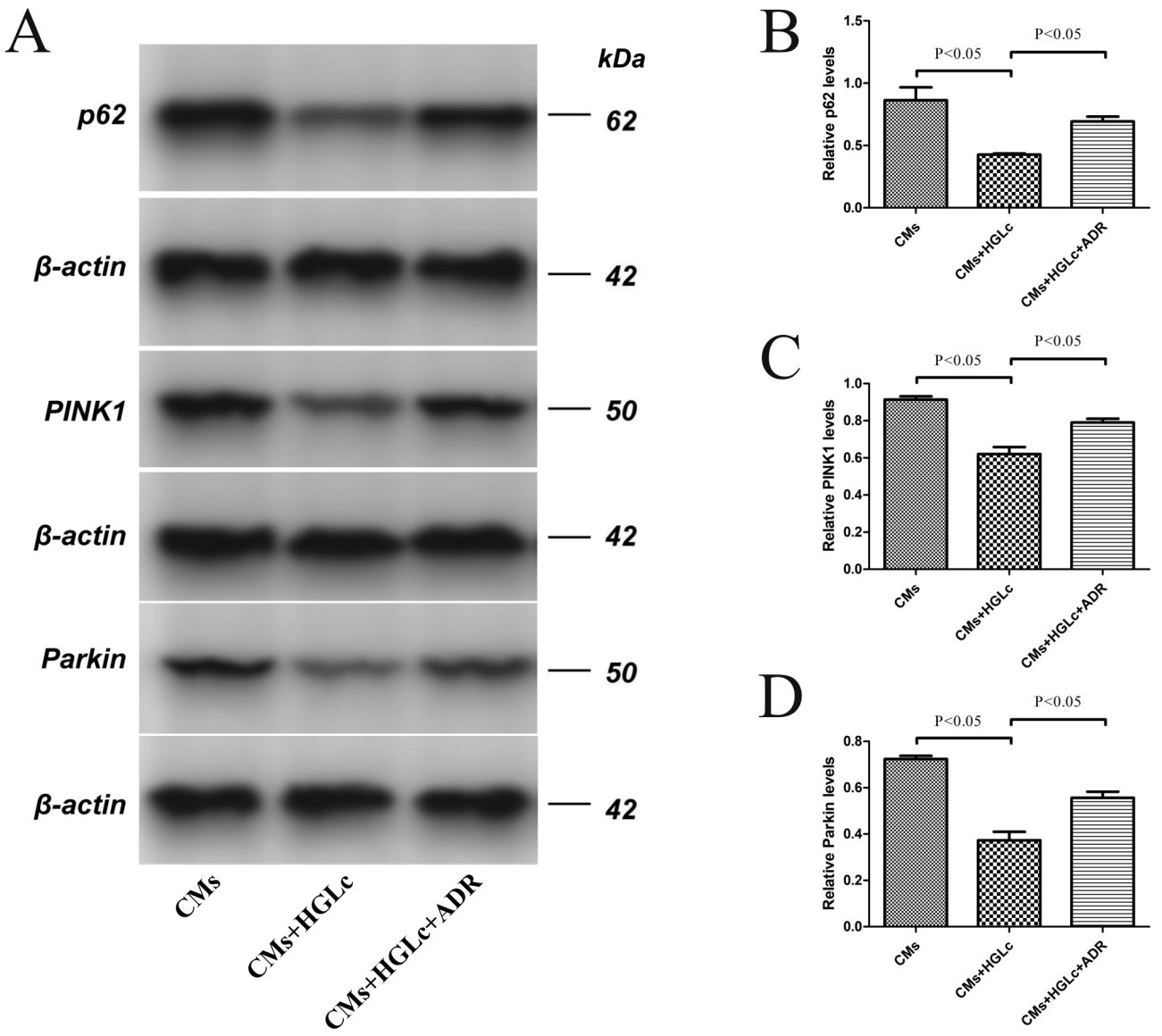

Fig. 6. Effect of ADR on mitophagy-related proteins in CMs. Mitophagy-related proteins were detected by Western blot. (A) Representative Western blot images showing the expression of mitophagy-related proteins [sequestosome 1 (p62), PTEN-induced kinase 1 (PINK1), Parkin] and and internal reference protein β-actin (molecular weight: p62: 62 kDa; PINK1: 50 kDa; Parkin: 50 kDa; β-actin: 42 kDa). From left to right: CMs group, CMs+HGLc group, CMs+HGLc+ADR group. (B) Quantitative analysis chart of relative p62 levels (normalized to β-actin). Compared with CMs group, the relative p62 level in CMs+HGLc group was decreased ($p < 0.05$); compared with CMs+HGLc group, the relative p62 level in CMs + HGLc + ADR group was increased ($p < 0.05$). (C) Quantitative analysis chart of relative PINK1 protein level (normalized to β-actin). Compared with the CMs group, the relative PINK1 level in the CMs + HGLc group was significantly decreased ($p < 0.05$); compared with the CMs + HGLc group, the relative PINK1 level in the CMs + HGLc + ADR group was significantly increased ($p < 0.05$). (D) Quantitative analysis chart of relative Parkin protein level (normalized to β-actin). Compared with the CMs group, the relative Parkin level in the CMs + HGLc group was significantly decreased ($p < 0.05$); compared with the CMs + HGLc group, the relative Parkin level in the CMs+HGLc+ADR group was significantly increased ($p < 0.05$). N = 3, it represents three independent biological replicates, with three technical replicates per experiment. Values were expressed as mean $\pm$ standard deviation.

we have extended previous *in vivo* findings and elucidated novel mechanisms of action. Our results demonstrate that ADR attenuates CM apoptosis and ameliorates myocardial remodeling in DbCM through modulation of mitochondrial dynamics and mitophagy - a previously unreported mechanism of ADR's cardioprotective effects. These findings not only provide the first evidence for ADR's regulation of mitophagy in CMs but also suggest its potential clinical

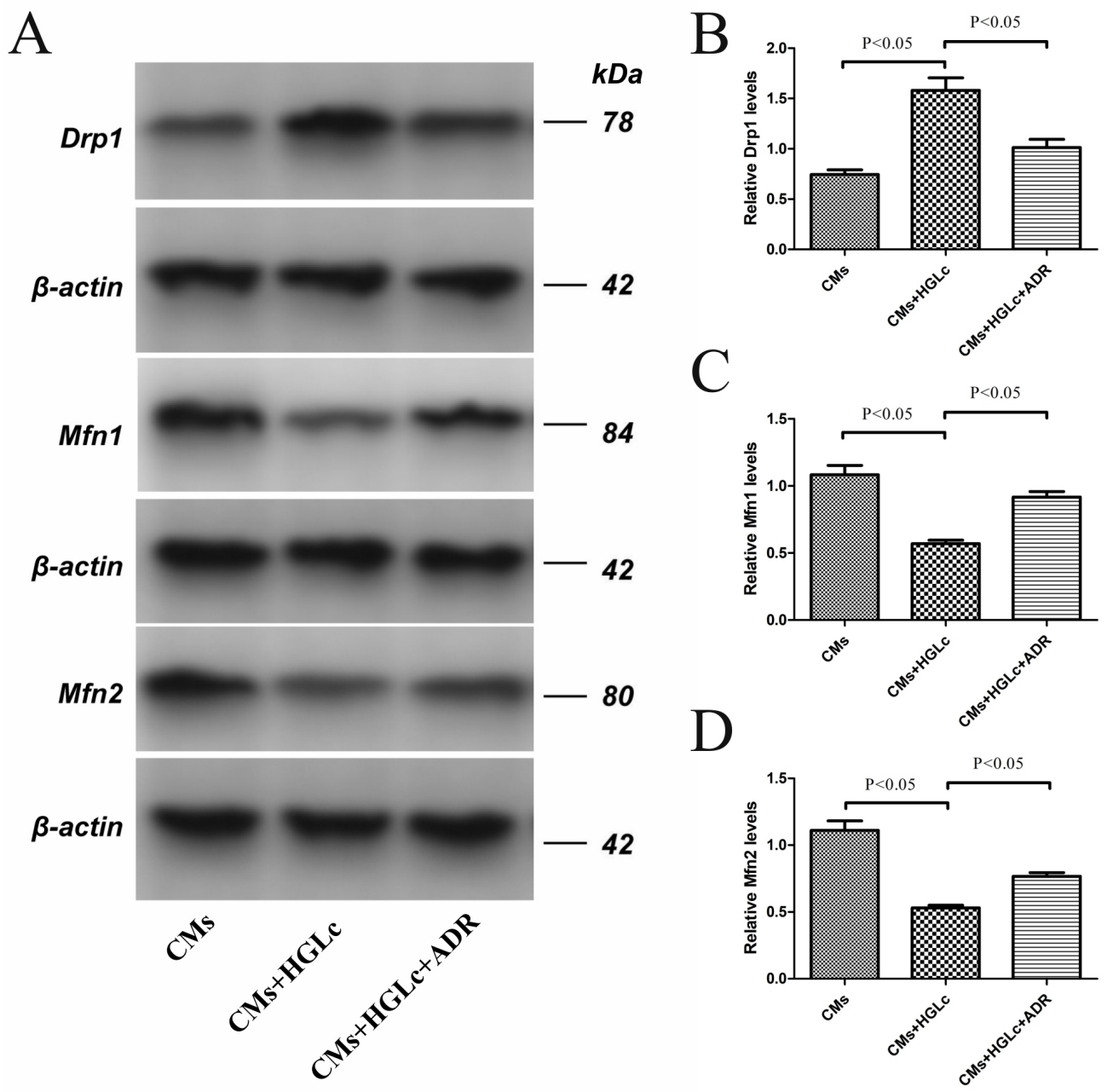

Fig. 7. Effect of ADR on mitochondrial dynamics - related proteins in CMs. Mitochondrial Dynamics-Related Proteins were detected by Western blot. (A) Representative Western blot bands of mitochondrial dynamics - related proteins [Dynamin-related protein 1 (Drp1), Mitofusin 1 (Mfn1), Mitofusin 2 (Mfn2)] and internal reference protein β-actin (molecular weight: Drp1: 78 kDa; Mfn1: 84 kDa; Mfn2: 80 kDa; β-actin: 42 kDa). From left to right: cardiomyocytes (CMs) group, CMs + high glucose condition (HGLc) group, CMs+HGLc+ adropin (ADR) group. (B) Quantitative analysis chart of relative Drp1 protein level (normalized to β-actin). Compared with the CMs group, the relative Drp1 level in the CMs+HGLc group was significantly increased ($p < 0.05$); compared with the CMs+HGLc group, the relative Drp1 level in the CMs+HGLc+ADR group was significantly decreased ($p < 0.05$). (C) Quantitative analysis chart of relative Mfn1 protein level (normalized to β-actin). Compared with the CMs group, the relative Mfn1 level in the CMs + HGLc group was significantly decreased ($p < 0.05$); compared with the CMs + HGLc group, the relative Mfn1 level in the CMs + HGLc + ADR group was significantly increased ($p < 0.05$). (D) Quantitative analysis chart of relative Mfn2 protein level (normalized to β-actin). Compared with the CMs group, the relative Mfn2 level in the CMs + HGLc group was significantly decreased ($p < 0.05$); compared with the CMs + HGLc group, the relative Mfn2 level in the CMs + HGLc + ADR group was significantly increased ($p < 0.05$). N = 3, it represents three independent biological replicates, with three technical replicates per experiment. Values were expressed as mean $\pm$ standard deviation.

utility in improving DbCM prognosis and treatment outcomes. However, several limitations should be acknowledged. However, this study also has some shortcomings. Firstly, ADR did not conduct experiments with different concentration subgroups. Besides, this study did not perform specific gene knockouts in exploring the mechanisms and bright-field microscopy imaging was not performed. Future studies will address these limitations to further characterize ADR's therapeutic potential.

5. Conclusion

In conclusion, ADR effectively attenuates cellular apoptosis through coordinated regulation of mitophagy and mitochondrial dynamics in high glucose-exposed CMs. These results position ADR as a promising therapeutic candidate for diabetic cardiomyopathy management, warranting further preclinical and clinical investigation.

Availability of Data and Materials

The datasets used and analyzed during the current study are available from the corresponding author on reasonable request.

Author Contributions

Conceptualization, ML and ZL; methodology, ML; software, PC; validation, PC, SW and ML; formal analysis, PC; investigation, SW; resources, ML; data curation, PC; writing—original draft preparation, PC; writing—review and editing, ML; visualization, GZ; supervision, ML; project administration, SW; funding acquisition, ML and ZL. All authors have read and agreed to the published version of the manuscript. All authors contributed to editorial changes in the manuscript. All authors have participated sufficiently in the work and agreed to be accountable for all aspects of the work.

Ethics Approval and Consent to Participate

All procedures involving animals were conducted in accordance with the ARRIVE (Animal Research: Reporting of In-Vivo Experiments) guidelines and National Institute of Health Guide for Care and Use of Laboratory Animals. And this study was conducted under the supervision of the Ethics Committee of North Sichuan Medical College.

Acknowledgment

The authors gratefully acknowledge the financial support from the Sichuan Provincial Medical Research Youth Innovation Project (Grant number: Q22063) and the Guang'an District People's Hospital Joint Development Research Project (Grant number: 2024LHFZ04).

Funding

The study was supported by Sichuan Provincial Medical Research Youth Innovation Project (Grant number: Q22063) and Guang'an District People's Hospital Joint Development Research Project (Grant number: 2024LHFZ04).

Conflict of Interest

The authors declare no conflict of interest.

References

[1] Sun H, Saeedi P, Karuranga S, Pinkepank M, Ogurtsova K, Duncan BB, *et al*. IDF Diabetes Atlas: Global, regional and country-level diabetes prevalence estimates for 2021 and projections for 2045. Diabetes Research and Clinical Practice. 2022; 183: 109119. https://doi.org/10.1016/j.diabres.2021.109119.

[2] Mehta A, Bhattacharya S, Estep J, Faiman C. Diabetes and Heart Failure: A Marriage of Inconvenience. Clinics in Geriatric Medicine. 2020; 36: 447–455. https://doi.org/10.1016/j.cger.2020.04.005.

[3] Nakamura K, Miyoshi T, Yoshida M, Akagi S, Saito Y, Ejiri K, *et al*. Pathophysiology and Treatment of Diabetic Cardiomyopathy and Heart Failure in Patients with Diabetes Mellitus. International Journal of Molecular Sciences. 2022; 23: 3587. https://doi.org/10.3390/ijms23073587.

[4] Zhao X, Liu S, Wang X, Chen Y, Pang P, Yang Q, *et al*. Diabetic cardiomyopathy: Clinical phenotype and practice. Frontiers in Endocrinology. 2022; 13: 1032268. https://doi.org/10.3389/fendo.2022.1032268.

[5] Hua Li, Xiao Cao, Jiejing Sun, Michelle Wang, Dandan Dong, Hao Wu. Inhibitory Effect of Astragalus membranaceus Extract on Myocardial Damage in Diabetes Complicated by Cardiomyopathy. International Journal of Pharmacology. 2024; 20: 1040–1050. https://doi.org/10.3923/ijp.2024.1040.1050.

[6] Yan T, Huang Y, Wu JHY, Zhuang XD, Pan XF. Editorial: Insulin Resistance, Metabolic Syndrome, and Cardiovascular Disease. Frontiers in Cardiovascular Medicine. 2022; 9: 959680. https://doi.org/10.3389/fcvm.2022.959680.

[7] Graczyk P, Dach A, Dyrka K, Pawlik A. Pathophysiology and Advances in the Therapy of Cardiomyopathy in Patients with Diabetes Mellitus. International Journal of Molecular Sciences. 2024; 25: 5027. https://doi.org/10.3390/ijms25095027.

[8] Abdullah AR, Seliem MA, Khidr EG, Sobhy AM, El-Shiekh RA, Hafeez MSAE, *et al*. A comprehensive review on diabetic cardiomyopathy (DCM): histological spectrum, diagnosis, pathogenesis, and management with conventional treatments and natural compounds. Naunyn-Schmiedeberg's Archives of Pharmacology. 2025; 398: 9929–9969. https://doi.org/10.1007/s00210-025-03980-9.

[9] Li B, Wang Z, He Y, Chen T, Zhang Y, Yuan X, *et al*. Adropin Improves Radiation-Induced Myocardial Injury via VEGFR2/PI3K/Akt Pathway. Oxidative Medicine and Cellular Longevity. 2022; 2022: 8230214. https://doi.org/10.1155/2022/8230214.

[10] Skrzypski M, Wojciechowicz T, Rak A, Krążek M, Fiedorowicz J, Strowski MZ, *et al*. The levels of adropin and its therapeutic potential in diabetes. The Journal of Endocrinology. 2025; 265: e240117. https://doi.org/10.1530/JOE-24-0117.

[11] Ali II, D'Souza C, Singh J, Adeghate E. Adropin's Role in Energy Homeostasis and Metabolic Disorders. International Journal of Molecular Sciences. 2022; 23: 8318. https://doi.org/10.3390/ijms23158318.

[12] Rooban S, Arul Senghor KA, Vinodhini VM, Kumar JS. Adropin: A crucial regulator of cardiovascular health and metabolic balance. Metabolism Open. 2024; 23: 100299. https://doi.org/10.1016/j.metop.2024.100299.

[13] Miao X, Alidadipour A, Saed V, Sayyadi F, Jadidi Y, Davoudi

M, *et al*. Hepatokines: unveiling the molecular and cellular mechanisms connecting hepatic tissue to insulin resistance and inflammation. Acta Diabetologica. 2024; 61: 1339–1361. https://doi.org/10.1007/s00592-024-02335-9.

[14] Soltani S, Beigrezaei S, Malekahmadi M, Clark CCT, Abdollahi S. Circulating levels of adropin and diabetes: a systematic review and meta-analysis of observational studies. BMC Endocrine Disorders. 2023; 23: 73. https://doi.org/10.1186/s12902-023-01327-0.

[15] Thapa D, Xie B, Zhang M, Stoner MW, Manning JR, Huckestein BR, *et al*. Adropin treatment restores cardiac glucose oxidation in pre-diabetic obese mice. Journal of Molecular and Cellular Cardiology. 2019; 129: 174–178. https://doi.org/10.1016/j.yjmcc.2019.02.012.

[16] Wei W, Liu H, Qiu X, Zhang J, Huang J, Chen H, *et al*. The association between serum adropin and carotid atherosclerosis in patients with type 2 diabetes mellitus: a cross sectional study. Diabetology & Metabolic Syndrome. 2022; 14: 27. https://doi.org/10.1186/s13098-022-00796-y.

[17] Berezin AA, Obradovic Z, Fushtey IM, Berezina TA, Novikov EV, Schmidbauer L, *et al*. The Impact of SGLT2 Inhibitor Dapagliflozin on Adropin Serum Levels in Men and Women with Type 2 Diabetes Mellitus and Chronic Heart Failure. Biomedicines. 2023; 11: 457. https://doi.org/10.3390/biomedicines11020457.

[18] Berezina TA, Berezin OO, Hoppe UC, Lichtenauer M, Berezin AE. Adropin Predicts Asymptomatic Heart Failure in Patients with Type 2 Diabetes Mellitus Independent of the Levels of Natriuretic Peptides. Diagnostics (Basel, Switzerland). 2024; 14: 1728. https://doi.org/10.3390/diagnostics14161728.

[19] Liu M, Ai J, Shuai Z, Tang K, Li Z, Huang Y. Adropin Alleviates Myocardial Fibrosis in Diabetic Cardiomyopathy Rats: A Preliminary Study. Frontiers in Cardiovascular Medicine. 2021; 8: 688586. https://doi.org/10.3389/fcvm.2021.688586.

[20] Tokuyama T, Yanagi S. Role of Mitochondrial Dynamics in Heart Diseases. Genes. 2023; 14: 1876. https://doi.org/10.3390/genes14101876.

[21] Chapa-Dubocq XR, Rodríguez-Graciani KM, Escobales N, Javadov S. Mitochondrial Volume Regulation and Swelling Mechanisms in Cardiomyocytes. Antioxidants (Basel, Switzerland). 2023; 12: 1517. https://doi.org/10.3390/antiox12081517.

[22] Zacharioudakis E, Gavathiotis E. Mitochondrial dynamics proteins as emerging drug targets. Trends in Pharmacological Sciences. 2023; 44: 112–127. https://doi.org/10.1016/j.tips.2022.11.004.

[23] Lin J, Duan J, Wang Q, Xu S, Zhou S, Yao K. Mitochondrial Dynamics and Mitophagy in Cardiometabolic Disease. Frontiers in Cardiovascular Medicine. 2022; 9: 917135. https://doi.org/10.3389/fcvm.2022.917135.

[24] Chen W, Zhao H, Li Y. Mitochondrial dynamics in health and disease: mechanisms and potential targets. Signal Transduction and Targeted Therapy. 2023; 8: 333. https://doi.org/10.1038/s41392-023-01547-9.

[25] Zhuang L, Jia K, Chen C, Li Z, Zhao J, Hu J, *et al*. DYRK1B-STAT3 Drives Cardiac Hypertrophy and Heart Failure by Impairing Mitochondrial Bioenergetics. Circulation. 2022; 145: 829–846. https://doi.org/10.1161/CIRCULATIONAHA.121.055727.

[26] Wu L, Fang J, Yuan X, Xiong C, Chen L. Adropin reduces hypoxia/reoxygenation-induced myocardial injury via the reperfusion injury salvage kinase pathway. Experimental and Therapeutic Medicine. 2019; 18: 3307–3314. https://doi.org/10.3892/etm.2019.7937.

[27] Mushala BAS, Scott I. Adropin: a hepatokine modulator of vascular function and cardiac fuel metabolism. American Journal of Physiology. Heart and Circulatory Physiology. 2021; 320: H238–H244. https://doi.org/10.1152/ajpheart.00449.2020.

[28] Ketenci M, Zablocki D, Sadoshima J. Mitochondrial Quality Control Mechanisms during Diabetic Cardiomyopathy. JMA Journal. 2022; 5: 407–415. https://doi.org/10.31662/jmaj.2022-0155.

[29] Zheng H, Zhu H, Liu X, Huang X, Huang A, Huang Y. Mitophagy in Diabetic Cardiomyopathy: Roles and Mechanisms. Frontiers in Cell and Developmental Biology. 2021; 9: 750382. https://doi.org/10.3389/fcell.2021.750382.

[30] Kobayashi S, Zhao F, Zhang Z, Kobayashi T, Huang Y, Shi B, *et al*. Mitochondrial Fission and Mitophagy Coordinately Restrict High Glucose Toxicity in Cardiomyocytes. Frontiers in Physiology. 2020; 11: 604069. https://doi.org/10.3389/fphys.2020.604069.

[31] Yapa NMB, Lisnyak V, Reljic B, Ryan MT. Mitochondrial dynamics in health and disease. FEBS Letters. 2021; 595: 1184–1204. https://doi.org/10.1002/1873-3468.14077.

[32] Peoples JN, Saraf A, Ghazal N, Pham TT, Kwong JQ. Mitochondrial dysfunction and oxidative stress in heart disease. Experimental & Molecular Medicine. 2019; 51: 1–13. https://doi.org/10.1038/s12276-019-0355-7.

[33] Jin JY, Wei XX, Zhi XL, Wang XH, Meng D. Drp1-dependent mitochondrial fission in cardiovascular disease. Acta Pharmacologica Sinica. 2021; 42: 655–664. https://doi.org/10.1038/s41401-020-00518-y.

[34] Quiles JM, Gustafsson ÅB. The role of mitochondrial fission in cardiovascular health and disease. Nature Reviews. Cardiology. 2022; 19: 723–736. https://doi.org/10.1038/s41569-022-00703-y.

[35] Tong M, Zablocki D, Sadoshima J. The role of Drp1 in mitophagy and cell death in the heart. Journal of Molecular and Cellular Cardiology. 2020; 142: 138–145. https://doi.org/10.1016/j.yjmcc.2020.04.015.

[36] Han H, Tan J, Wang R, Wan H, He Y, Yan X, *et al*. PINK1 phosphorylates Drp1^{S616} to regulate mitophagy-independent mitochondrial dynamics. EMBO Reports. 2020; 21: e48686. https://doi.org/10.15252/embr.201948686.